JOURNAL OF MATERIALS SCIENCE 20 (1985) 563–577

Toughening of polyester resins by rubber modification

Part 2 *Microstructures*

G. A. CROSBIE, M. G. PHILLIPS
School of Materials Science, University of Bath, Claverton Down, Bath, UK

The microstructures of two polyester resin systems, with reactive liquid rubber additions incorporated, were investigated using electron microscopy. Fracture surface morphologies of failed fracture toughness specimens were examined using scanning electron microscopy. The fine structures of unfractured toughened resins were examined by imaging ultra thin sections in the transmission electron microscope. Three of the four rubber additives investigated produced, upon curing, a dispersion of second-phase rubber-rich particles in the polyester resin matrix. The fourth additive, which was more compatible with polyester than the other three, did not produce any detectable particle dispersion upon curing, even at relatively high concentrations. The fine structures of the particle distribution were found to be highly dependent upon both rubber and resin formulations. Rubber additions modified the mode of fracture observed in double torsion tests of polyester resins, from continuous crack propagation to "slip–stick", and distinctive changes in fracture surface morphology were observed. In zones of crack arrest and slow stable crack growth, crack blunting occurred and highly deformed structures were seen on the fracture surface. In one system, this zone was split into two distinct regions, due to crack blunting and the initiation of new, sharp cracks. In zones of rapid crack growth, there was no evidence of crack blunting. The amount of crack blunting was highly dependent upon speed of testing.

1. Introduction

The incorporation of second-phase elastomer particles into brittle resins has long been known to have a beneficial effect upon their fracture resistance, and microstructural studies have proved useful in explaining the toughening action of these particles [1]. Using transmission electron microscopy on replicas from polished and etched sections, Sultan and McGarry showed that fine second-phase particles, with heterogeneous internal structures, are formed when polyester resins are modified with reactive liquid rubbers [2]. They applied a similar technique to rubber-toughened epoxy resin [3] but found that no particular substructure was revealed. They also used scanning electron microscope (SEM) fractography on toughened epoxies, and this provided useful data on crack–particle interactions, during fracture.

More recently, SEM fractography has yielded information on how rubber dispersions modify the mode of fracture of thermosets, both in bulk materials [4] and in adhesive joints [5]. The aim of this study was to characterize the structures of the rubber toughened polyester, whose mechanical properties are described in Part 1 of this paper [6], and to relate the observed differences in structure to the changes in the properties.

2. Materials and experimental procedure

Details of the polyester resin and reactive liquid polymer rubber systems examined in this investigation are given in Part 1 of this paper [6]. Microstructures of the rubber–resin systems, and the

0022–2461/85 $03.00 + .12

fracture surface morphologies of specimens tested in double torsion were studied using scanning and transmission electron microscopy (SEM and TEM).

Fracture surface morphologies were examined using a Jeol 35c SEM. Sections of fracture surfaces, around 20 mm long, were cut from double torsion specimens. Care was taken to minimize the amount of cutting debris which came into contact with the surface to be examined. Any debris on the surface was washed off using distilled water; it was not possible to use organic solvents for this purpose, because they attack the rubber-rich phases. The sections were then attached to 25 mm wide aluminium stubs, using a conductive colloidal silver dag, and a thin layer of gold (around 50 nm) was vacuum sputtered on to them, so that they would be electronically conductive in the SEM.

Ultra thin sections of rubber-toughened resin were examined in a Jeol 100c TEM. Specimens were first trimmed up on an ultramicrotome to form truncated pyramids of undeformed material, the top surfaces of which were approximately 1 mm square. The blocks were then stained, using a technique developed by Riew and Smith for staining rubber-toughened epoxies [7]. Samples were immersed in a 1% weight/volume solution of osmium tetroxide crystals in tetrahydrofuran. The metal salt preferentially fixed regions of chemical unsaturation, so that they became electron opaque and would slow up as darkened regions in the TEM. Tetrahydrofuran gives greatly improved penetration of the fixing agent into the resin, compared with aqueous osmium tetroxide solutions [7]. Immersion for 10 min was found to give a stained layer around 20 μm deep, from which was cut a number of sections, around 100 nm thick, using a diamond knife. These were collected on a 3mm copper grid, ready for insertion in the TEM.

3. Results

3.1. Effects of different modifying rubbers

Three of the four rubber additives produced distributions of second-phase particles in polyester, in the two resin systems examined. CTBN, VTBN and CRC modified resins contained particle distributions at all levels of modification examined; in HTE modified resins, no second-phase particles were seen up to 15 pph rubber content. Fig. 1 shows scanning electron micrographs of fracture surfaces from double torsion (DT) specimens of C392 resin, modified with different reactive liquid rubbers. The magnifications of the photographs are indicated by the scale bar at the bottom right of each figure, the bar length being given in μm. In CTBN, VTBN and CRC modified systems, shown here modified to 2 pph rubber (Figs. 1a to c), the particles appeared as nearly circular features in the size range 1 to 10 μm. Particle morphologies on the fracture surface appeared different for each rubber modifier. In contrast, C392 resin combined with HTE rubber showed no such features, even when modified to 15 pph (Fig. 1d), and fracture surface morphologies resembled those seen in unmodified C392 resin (Fig. 1e).

Similar trends were seen in rubber-modified C600PA resin. CTBN and CRC rubber additions gave rise to distributions of particles of similar size range to those seen in modified C392 resin, at all levels of modification investigated. VTBN toughened C600PA resin specimens were not examined. In HTE-modified C600PA resin, again no second-phase particles were seen, up to 15 pph modifier content.

HTE rubber has been developed to give a higher degree of chemical compatability with polyester resins in the uncured state, than does the commercially available butadiene acrylonitrile-based rubber, so that it can easily be dissolved in liquid resin prior to curing. A possible explanation of our observations is that the degree of compatibility of HTE rubber with C392 and C600PA resins was too great, and that the resin and rubber cured together to form a single-phase, homogeneous mixture, rather than a multi-phase structure containing discrete rubbery domains.

One must, of course, admit the possibility that with HTE rubber a dispersion does form, but on a scale too fine to be resolved in the SEM. Unfortunately, HTE rubber fails to respond to the staining treatment used for our higher-resolution TEM work (see Section 3.2), so that this cannot provide conclusive evidence either. Our assessment of these structures as single-phase can only be tentative, therefore.

Other workers [8, 9] have found CTBN and VTBN rubbers to be insufficiently compatible with polyester resins, in the uncured state, to give fine particle distributions upon curing. These rubbers are soluble in uncured resins only to low levels of modification, and rapidy separate out to form an emulsion of coarse rubbery globules in the liquid resin, if higher levels of modification are attempted [8]. Fig. 2a shows a scanning electron

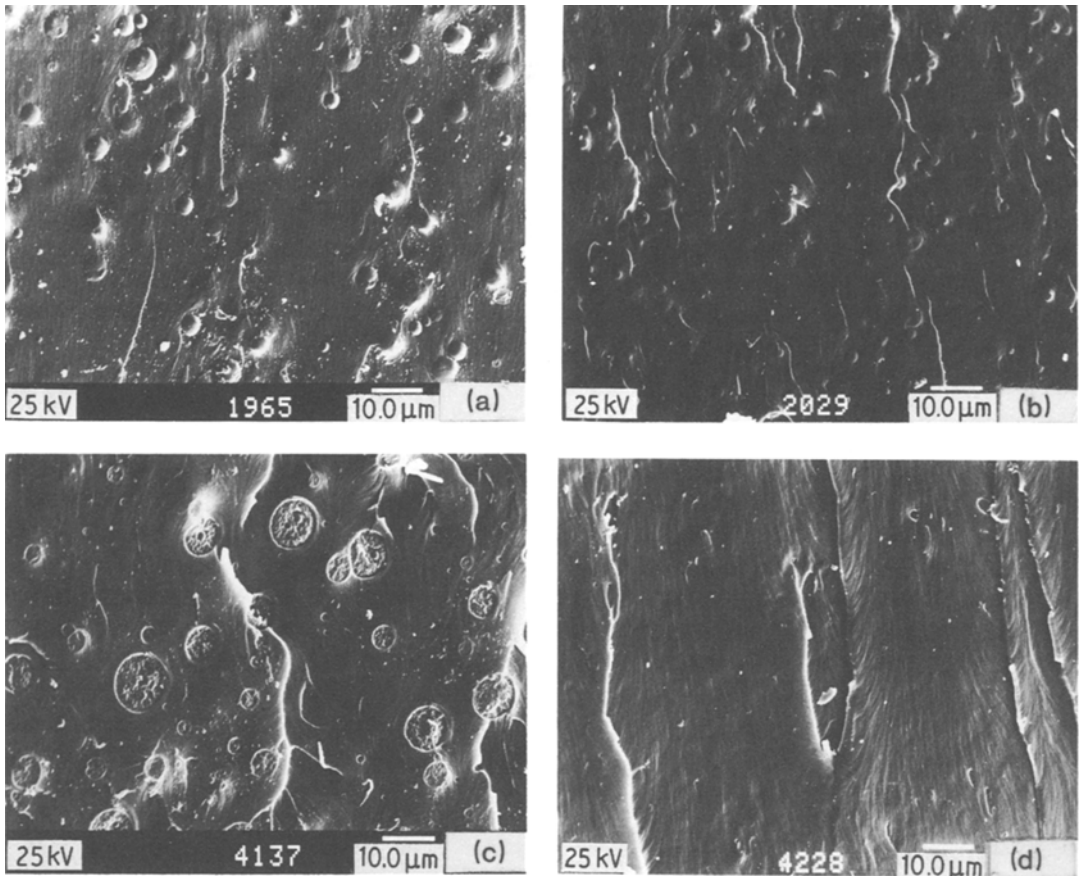

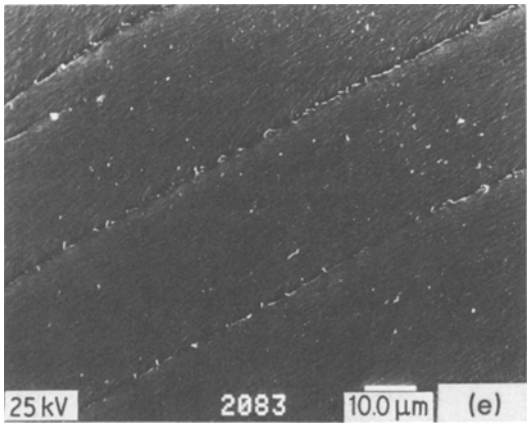

Figure 1 Scanning electron micrographs of DT fracture surfaces for C392 resin, modified with (a) 2 pph CTBN, (b) 2 pph VTBN, (c) 2 pph CRC, (d) 15 pph HTE, (e) unmodified.

micrograph from a fracture surface of C392 resin, modified with 10 pph CTBN rubber. The second-phase particles were much coarser than any of those found in Fig. 1, and were generally in the size range 10 to 50 μm, although some particles of up to 100 μm diameter were present. Particles of this size range have been found to be less efficient at toughening thermoset resins than those of the type seen in Fig. 1 [8], so it may be concluded that modifications with CTBN and VTBN rubbers to this level will not produce large improvements in resin toughness, under normal curing conditions, because of poor resin–rubber compatibility.

Resin modification to around 10 pph rubber content was, however, no problem with CRC rubber. CRC rubber was readily soluble in uncured resin, up to this level of modification, and it did not separate from the resin prior to the curing reaction occurring. Fig. 2b shows a fractograph of a C392 resin sample modified with 9 pph CRC rubber. Photographs in Fig. 2 are all at similar magnifications, and differences in microstructure between Figs. 2a and b are immediately apparent. The CRC modified structure was much more homogeneous, and contained a uniform dispersion of smaller second-phase particles, of size range 2 to 10 μm.

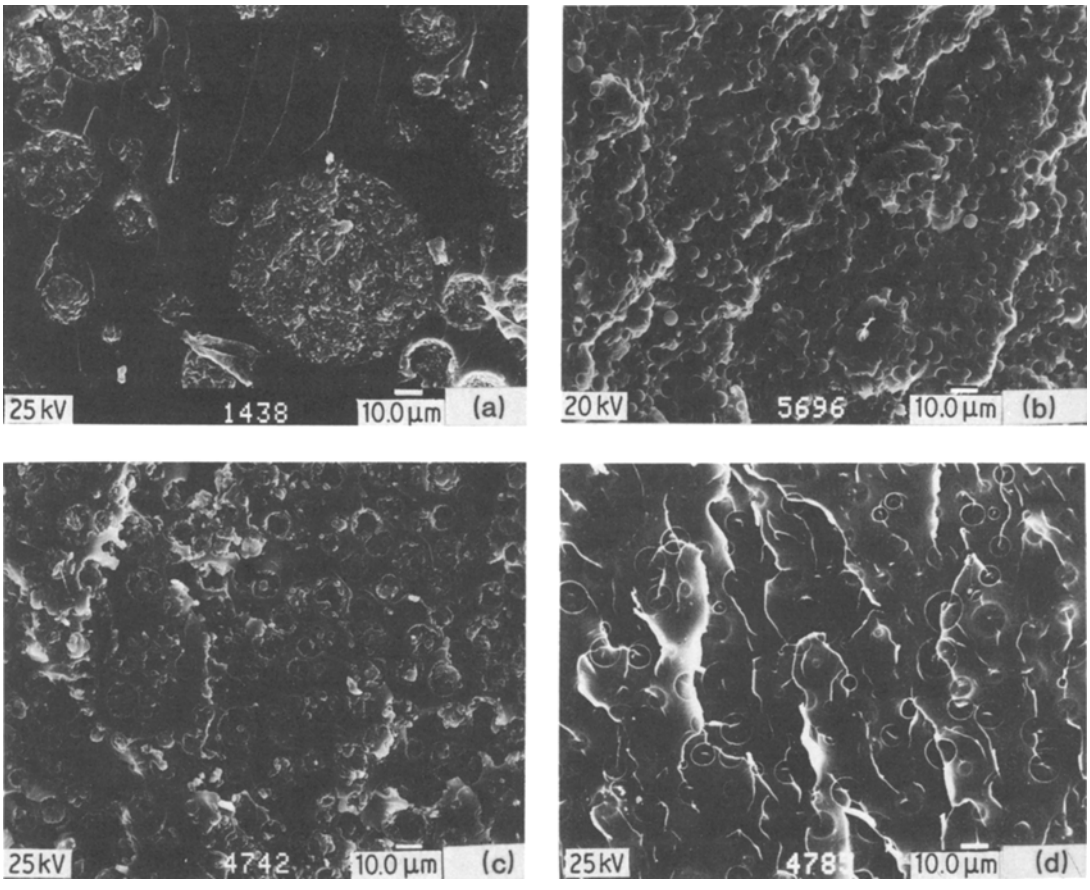

Figure 2 Scanning electron micrographs of DT fracture surfaces for C392 resin, modified with (a) 10 pph CTBN, (b) 9 pph CRC, (c) 10 pph CTBN, "hot-poured", (d) 10 pph VTBN "hot-poured".

Relatively fine and homogeneous distributions of rubber particles can be produced in polyester resins, with CTBN and VTBN rubber additives, if suitable curing conditions are used. In the course of this investigation it was found that, although these rubbers are relatively immiscible with polyester resins at ambient temperatures, they will dissolve in warm resin, to much higher modifer contents, without forming coarse globular emulsions. By heating the resin to 60° C it was found that 10 pph CTBN or VTBN could be dissolved, and that catalysing the mixture after cooling to 40° C gave enough time for the resin plaques to be cast without gross separation of the rubber from the resin. Fractographs of these "hot-poured" microstructures are shown in Figs 2c and d. In both CTBN and VTBN modified polyesters, the particle distributions were finer and more homogeneous than those seen in cold-cured polyester (shown in Fig. 2a at similar magnification), but they were still coarser than those seen in the CRC-modified resin (Fig. 2b). In the CTBN-modified resin, particles were generally in the size range 10 to 15 μm. In VTBN modified polyester, some particles were smaller, and particle diameters ranged from around 5 to 15 μm. Fig. 2 clearly shows the differences in particle morphologies which occur in the different modifying systems. These distributions gave improvements in fracture toughness which were greater than those seen in less heavily modified polyester. In C392 resin modified with 10 pph CTBN the fracture surface energy for crack initiation (G_i) was found to be 825 J m^{-2}, using the double torsion test at 1 mm min^{-1} crosshead speed [6]. This represents more than an eight-fold increase compared with the base resin toughness ($G_i = 95$ J m^{-2}), and is comparable with the toughening effect obtained in CRC modified resins, with similar rubber contents [6]. In C392 resin, modified with 10 pph VTBN, the improvement in toughness was less pronounced, and G_i increased to 225 J m^{-2}.

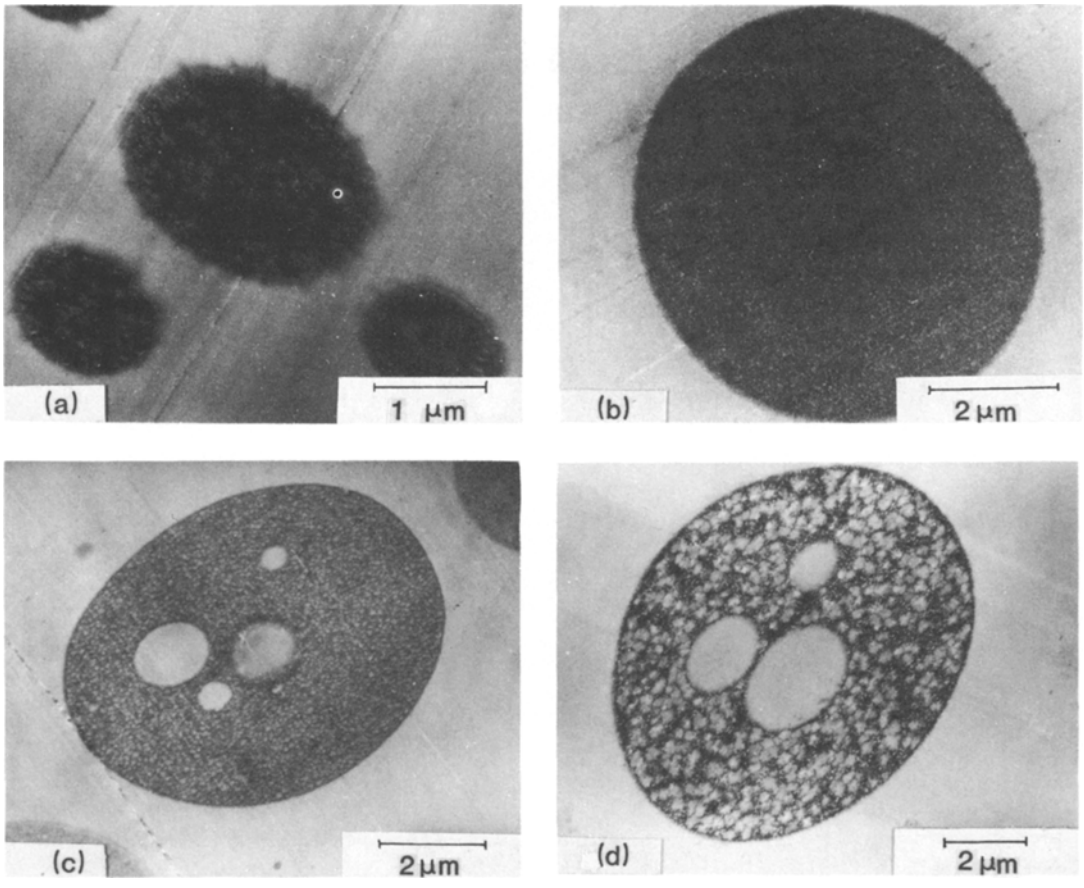

Figure 3 Transmission electron micrographs of stained ultra thin sections of rubber modified resins (a) C600PA + 3 pph CTBN; (b) C392 + 10 pph VTBN; (c) C392 + 9 pph CRC; (d) C600PA + 9 pph CRC.

3.2. Microstructure of particles

SEM fractography has proved useful for studying rubber particle distributions in resins, but it cannot give detailed information on the internal structure of the particles. For this purpose, transmission electron microscopy (TEM) of stained ultra thin sections has been employed. Sections for examination were taken from pieces of undeformed modified resin. Prior to sectioning, these had been stained with osmium tetroxide, to reveal areas of chemical unsaturation [7]. The polyester resins investigated were unsaturated in the uncured form, but the curing reaction and subsequent post-curing cross-linked the polyester chains with styrene, at the unsaturated sites on the dibasic acid. This left the resin saturated, so it was not expected to stain under the action of osmium tetroxide. The rubbers contained unsaturated sites and were therefore dark staining in the presence of osmium tetroxide, giving good contrast with the resin matrix. HTE rubber was, however, an exception, as it was fully saturated. HTE rubber distributions could not be examined using this technique.

3.2.1. CTBN particles

Fig. 3a shows a transmission electron micrograph of CTBN rubber particles from a C600PA resin plaque, modified with 3 pph CTBN rubber. The background resin is electron transparent, indicating little or no residual chemical unsaturation in the matrix, whereas the rubber-rich particles are stained dark, due to the presence of unsaturated sites. In the micrograph, the particles do not appear circular, and this may be attributed to deformation of the rubbery domains during sectioning [1]. The direction of sectioning is indicated by the diagonal streaks across the micrograph, and particle deformation has occurred perpendicular to these knife marks. The particles are

not single-phased and homogeneous, but have a dual-phased structure, with the rubber-rich phase etching darker. The diffuse nature of the particle–matrix interface, with its gradually decreasing degree of saturation, indicates that rubber–resin grafting may be occurring across the interface, giving some degree of bonding of the particles to the surrounding matrix [10].

3.2.2. VTBN particles

Fig. 3b, which is at lower magnification than Fig. 3a shows a rubber particle in a C392 resin plaque, modified with 10 pph VTBN rubber. In this specimen, sectioning has caused only slight distortion of the particle shape. The particle is more homogeneous than those seen in CTBN-modified resins, and any particle structure which may be present is difficult to resolve. It does seem, however, that there may be a very fine dual-phased substructure in the particle, with the majority of the particle volume being made up of the rubbery phase, finely interspersed with saturated material. The proportion of saturated material appears to be much less than one-half.

3.2.3. CRC particles

Figs. 3c and d show CRC particles in C392 and C600PA resins, modified with 9 pph CRC rubber. Again, the particles do not appear circular, because of distortion during sectioning. In both resin systems, the particles are multi-phased, containing saturated phases in two distinct morphologies. Firstly there are large occluded regions of saturated material, often in excess of 1 μm diameter, in the centre of the particles. These regions are distorted in the same direction as the particle and one may, therefore, assume that they were approximately spherical in particles which had not suffered sectioning deformation. Secondly, the saturated material occurs as a dispersion throughout the particle, intimately mixed with the rubber phase. In both cases, the proportion of saturated material in this mixture appears to exceed one-half. The two different resins systems do, however, show distinct differences in the morphology of this material. In C392 resin (Fig. 3c) the saturated phase is dispersed homogeneously throughout the rubbery phase, in a fine, uniform distribution. In C600PA resin (Fig. 3d), saturated colonies are more heterogeneously distributed, and show a range of sizes. Overall, the saturated domains are larger than those seen in C392 resin, but there also appears to be some fine substructure of saturated regions within the unsaturated rubber-rich phase. In both systems, there is a continuous rubber-rich region around the outside of the particles, with some evidence of a diffuse grafting layer at the particle–resin interface. From this detailed structural evidence, it may be concluded the chemistry of both the resin and the modifying rubber have an important effect upon particle distributions and morphologies.

3.3. Effect of rubber content upon particle distribution

In all of the rubber–resin systems investigated, except for HTE-modified polyester, the rubber particle distribution was affected by the amount of rubber added. Fig. 4 shows C392 resin toughened with increasing amounts of CRC rubber, respectively 2 pph (Fig. 4a) 4 pph (Fig. 4b) 9 pph (Fig. 4c). Magnification is the same in all cases. It is evident there are at least two parameters influencing the microstructure: particle count and particle size. It is natural to expect that the volume fraction of particles will increase with the rubber content, but the situation is complicated by the heterogeneous nature of the particles, and the fact that their number may vary independently of rubber content, because of the random nature of the nucleation process. One may attempt to analyse this in the following way. If it is assumed first that all the added rubber is present in particles, and second that its density is the same as the bulk rubber then the volume fraction of rubber, v_r, is related to the modifier content in parts by weight per hundred parts of resin (w_r) by the expression

$$v_r = 1 \Big/ \left(1 + \frac{100}{w_r} \times \frac{d_r}{d_m}\right),$$

where d_r and d_m are densities of rubber and polyester matrix, respectively.

Within each particle, as has been seen above, there exist regions of saturated material. If these too are assumed to contain no rubber, they may be regarded as sub-inclusions, expanding the volume fraction of particles (v_p) for a constant value of v_r. If within the particles there is a fraction f of sub-inclusions, then v_p is related to v_r by the expression

$$v_p = v_r/(1-f).$$

It is impossible to measure f directly, since it may

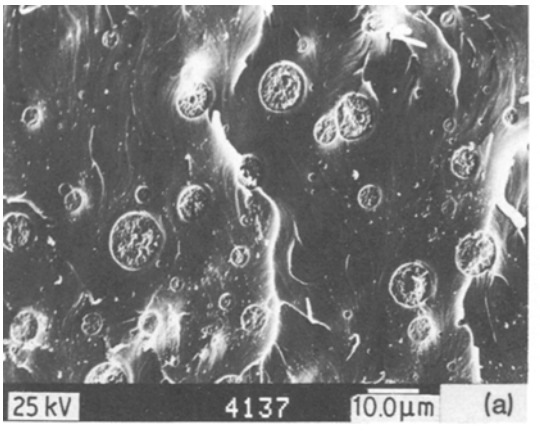

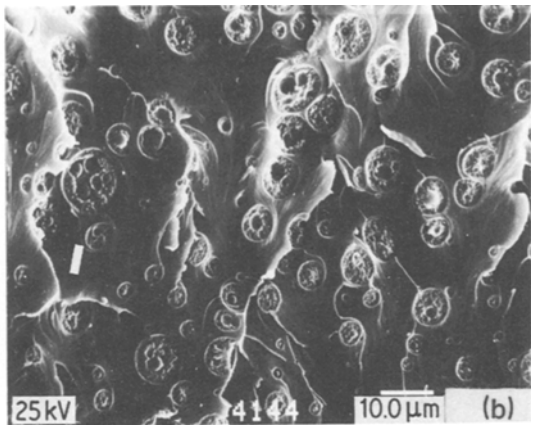

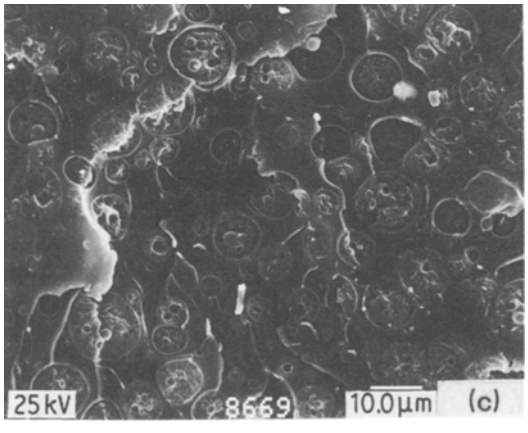

Figure 4 Scanning electron micrographs of DT fracture surfaces for C392 resin, modified with (a) 2 pph CRC, (b) 4 pph CRC, (c) 9 pph CRC.

vary from particle to particle, but an estimate may be made in individual cases, as has been done from Fig. 3 above. In an attempt to rationalize the microstructures presented in Fig. 4, estimates of v_p and v_r have been made, and the corresponding values of f determined. Results are given in Table I.

Each micrograph represents a single sample of the relevant structure. As a fracture surface is neither flat nor randomly selected it may not be truly representative. Therefore, the quantitative assessments to be made are subject to large errors. Parameters reported in Table I are: the calculated volume fraction of rubber, v_r; the particle count (total number of particles within the field of view); mean particle diameter (which embraces variations due to non-diametral sectioning of particles, as well as those due to variations in absolute size); the estimated particle volume fraction, v_p (actually the area fraction of particles in the chosen section which, as is shown in standard works on quantitative microscopy, is an unbiased estimate of the volume fraction); and finally the calculated fraction of sub-inclusions, f, for the particles.

It will be seen that on passing from 2 to 4 pph modifier, there is a sharp increase in the number of particles, but little change in their average size. Further increase of additive to 9 pph causes a notable increase in the mean particle size, but not much change in the particle count. A consistent trend is revealed, however, by examining the total volume fraction of particles.

There further appears to be some consistency in the structure of the particles as composition varies, because the calculated fraction of sub-inclusions is almost constant over this range of compositions.

TABLE I Parameters derived from the micrographs of Fig. 4

Additive content (pph)	Volume fraction of rubber, v_r*	Particle count †	Mean particle diameter (μm)	Particle volume fraction, v_p	Fraction of sub-inclusions f ‡
2	0.025	35	4.5	0.09	0.72
4	0.050	76	4.4	0.21	0.76
9	0.106	82	5.9	0.28	0.71

*Assumes zero solubility of rubber in resin. $d_r = 0.95$, $d_m = 1.25$.
†Total within field of view.
‡Calculated values. See text.

Recalling that these are, in fact, areas of saturated resin constituent, the calculated f of around 70% in these particles of CRC in C392 resin is consistent with the appearance of the single particle in Fig. 3c. Similar features are observed for CTBN rubber in this same resin. Figs. 2a and c show a large disparity between particle volume fraction and calculated rubber volume fraction, because of sub-inclusions in the particles. In similar vein, the volume fraction of VTBN rubber particles in C392 resin (Fig. 2d), approaches much more closely to the calculated volume fraction of rubber, because the particles are more homogeneous, as Fig. 3b confirms.

3.4. Effect of testing speed on fracture surface morphology

In resins modified with CTBN, VTBN and CRC rubbers and tested in double torsion, the crack propagation subsequent to initiation was not continuous. Instead, discontinuous "slip–stick" propagation occurred [6], and this gave rise to distinctive fracture surface features. Whereas, on a macroscopic level, few features were visible on the fracture surface of specimens which failed in a continuous manner, those which failed by "slip–stick" showed very distinct crack arrest zones. The overall shape of the arrest zones was dependent upon the test geometry, but their width and appearance were a function of rubber type, rubber content and speed of testing. In all cases, stress whitening had occurred in the arrest zones, but the degree of whitening was also dependent upon the aforementioned factors. In CRC-toughened resins, whitening was much more pronounced than in CTBN-toughened material; VTBN-modified polyester showed only slight stress whitening. Generally, at higher rubber contents, the width of the arrest zone and the intensity of stress whitening both increased.

Fig. 5 shows sections of DT crack arrest zones in C392 resin, toughened with 9 pph CRC rubber and tested over three decades of crosshead speed (0.1 to 100 mm min^{-1}). The arrest zones appeared as curved bands of stress whitened material, surrounded by relatively featureless regions where rapid crack propagation has occurred. The width of the arrest zone was highly dependent upon speed of testing. At the lowest crosshead speed, 0.1 mm min^{-1}, the arrest zone was in excess of 1 mm wide, whereas at the highest speed, 100 mm min^{-1}, this width was reduced to around 0.25 mm. The complex nature of the DT test geometry made it difficult to assign a precise value to arrest zone width, as it was dependent upon the position on the specimen where it was measured. Fig. 5 also shows that, at all but the fastest speed of testing, two distinct regions were visible within the arrest zones, zone I and zone II. These regions are most immediately apparent in Fig. 5a, but they can also be seen in Figs. 5b to d. The cracks, which propagated from right to left in Fig. 5, formed zone I, which appears at the bottom of the region, and is associated with deformation and fracture processes which had occurred in the early stages of the crack arrest period. Zone II which appears at the top of the arrest region, is also formed, and this is associted with processes which had occurred in the later stages of arrest or prior to the recommencement of rapid crack propagation. Since the size of the arrest zone and the degree of stress whitening occurring in it was so dependent upon speed of testing, it may be concluded that the deformation processes occurring in the zone were highly time-dependent.

3.5. Rapid crack propagation and crack arrest

3.5.1. CRC-toughened resins

Fig. 6 shows detail of the fracture surface morphologies of the three distinct regions visible in Fig. 5, for C392 resin with additions of 9 pph. CRC rubber. Fig. 6a shows the region of rapid crack propagation. At low magnification, this region appeared relatively flat and featureless, and at the higher magnification it is apparent that there is little perturbation of the fracture path, by the rubber particles. In nearly all cases, the crack path passed through the particles, but in a few, the fracture path has followed the particle–resin interface.

Fig. 6b shows zone I of crack arrest. This region was very rough, compared with the region of rapid cracking, and there was considerable localized variation in the plane of cracking. In this region, the crack path cut through the particles in all cases, but the particle appearance was different from that seen in Fig. 6a. Particles had a more deformed appearance, and even at this magnification, some of the internal structure of the particle could be seen. Fig. 6c shows zone II of the crack arrest region. The appearance of the fracture surface in this region is different from that seen in Figs. 6a and b. The fracture surface was again

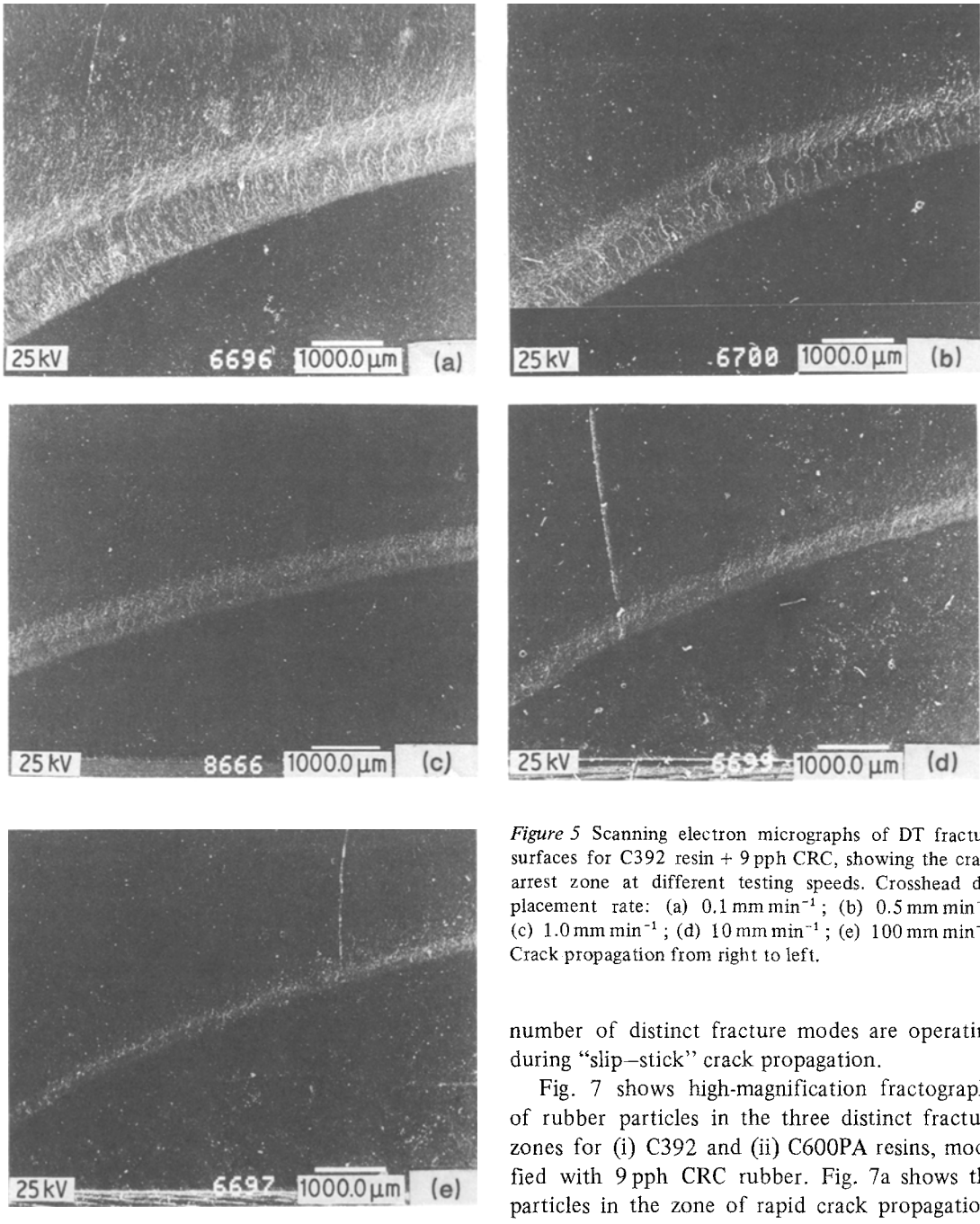

Figure 5 Scanning electron micrographs of DT fracture surfaces for C392 resin + 9 pph CRC, showing the crack arrest zone at different testing speeds. Crosshead displacement rate: (a) 0.1 mm min^{-1}; (b) 0.5 mm min^{-1}; (c) 1.0 mm min^{-1}; (d) 10 mm min^{-1}; (e) 100 mm min^{-1}. Crack propagation from right to left.

rougher than in the region of rapid cracking, but the rubber particle morphology was different. The crack path passed around the particles in nearly all cases, rather than cutting through them. In Fig. 6c particles stand out from the fracture surface, and the concave sites, where particles have been embedded in the resin prior to fracture, are also clearly visible. These observations indicate that a number of distinct fracture modes are operating during "slip–stick" crack propagation.

Fig. 7 shows high-magnification fractographs of rubber particles in the three distinct fracture zones for (i) C392 and (ii) C600PA resins, modified with 9 pph CRC rubber. Fig. 7a shows the particles in the zone of rapid crack propagation. In both resin systems, the particles were fractured with no deviation of the crack path occurring. There was no evidence of plastic deformation of the particles, either internally or at the particle–resin interface, in either of the resin systems. The difference in structure of the rubber particles in the two resin systems is clearly visible, the particles in C600PA resin being internally coarser than those in C392 resin.

Fig. 7b shows high-magnification of frac-

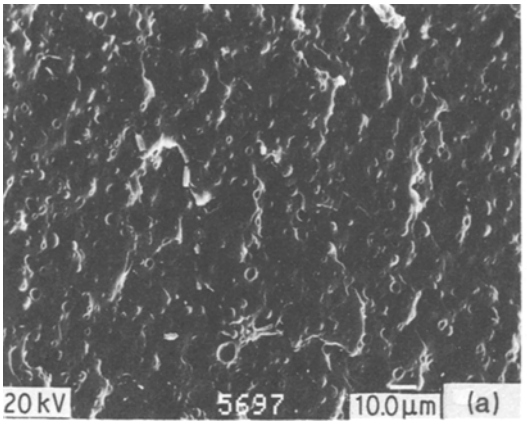

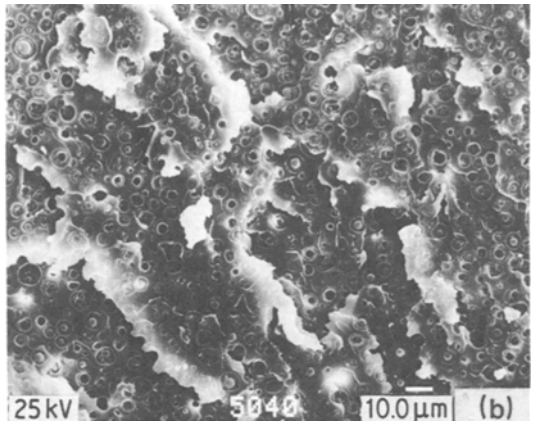

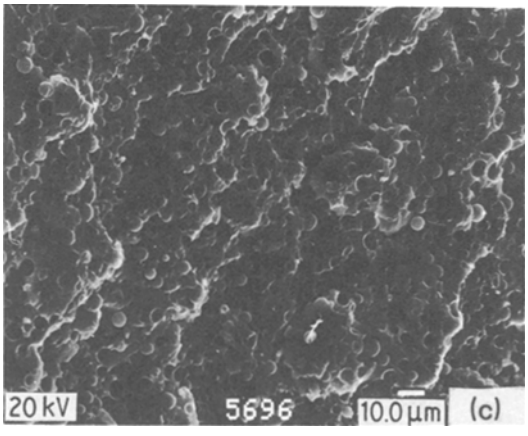

Figure 6 Scanning electron micrographs of DT fracture surface for C392 + 9 pph CRC, tested at 0.1 mm min^{-1} crosshead displacement speed. Micrographs show (a) fast fracture zone, (b) arrest zone I, (c) arrest zone II.

tographs of particles in zone I. Again, most of the particles fractured in both resin systems. There was, however, a higher incidence of failure at the resin–particle interface in particles in C600PA resin than there was in C392, in zone I (Fig. 7b (ii)). The major difference between fracture surfaces in the fast fracture zone, and in zone I was that there was considerable decohesion and cavitation at the particle–matrix interface in the latter case. In C392 resin, a gap of around 200 nm had opened up around the particles, at the particle–matrix interface; in C600PA this gap was larger (200 to 400 nm). The particles remained attached to the matrix by radial ligaments of the rubbery phase, which stretched from the particle surface to the matrix. These ligaments were finer in C392 resin than they were in C600PA, in line with the general trend of differences in structure between particles in the two resin systems.

Fig. 7c shows high-magnification fractographs of particles in zone II of the arrest zone. In this region, there was little evidence of particle fracture and in nearly all cases, failure occurred at the resin–matrix interface. Again, there was a region of decohesion and void formation at the particle–matrix interface, and around some particles this gap exceeded 500 nm in width. The rubbery ligaments, by which the particles remained attached to the resin matrix were visible in both resin systems; they were coarser and more pronounced in C600PA resin. The overall appearance of the rubber particles embedded in the fracture surface was different in the two resin systems. In C392 resin, the particles in this region had relatively smooth surfaces, whereas in C600PA resin, they had a granular, uneven appearance. In Fig 7c (ii) there is clear evidence that some of the rubber-rich phase has remained attached to the resin matrix, during plastic deformation.

3.5.2. CTBN-toughened resins

Fig. 8a shows a section of the DT crack arrest zone in C600PA resin, toughened with 3 pph CTBN rubber, tested at a crosshead speed of 1 mm min^{-1}. In this photograph, the direction of crack propagation is from left to right. Stress whitening in the arrest zone was less pronounced than in the CRC-toughened resin of similar rubber content, tested at the same speed. The arrest zone was also narrower, around 50 μm, compared with 300 μm in the equivalent CRC-toughened resin. There was no visible subdivision of the arrest zone into zones I and II as was seen in CRC-toughened resin.

Detail of the regions of fast fracture and crack arrest is shown in Figs. 8b and c. The fast fracture region was flatter than the arrest zone, and the

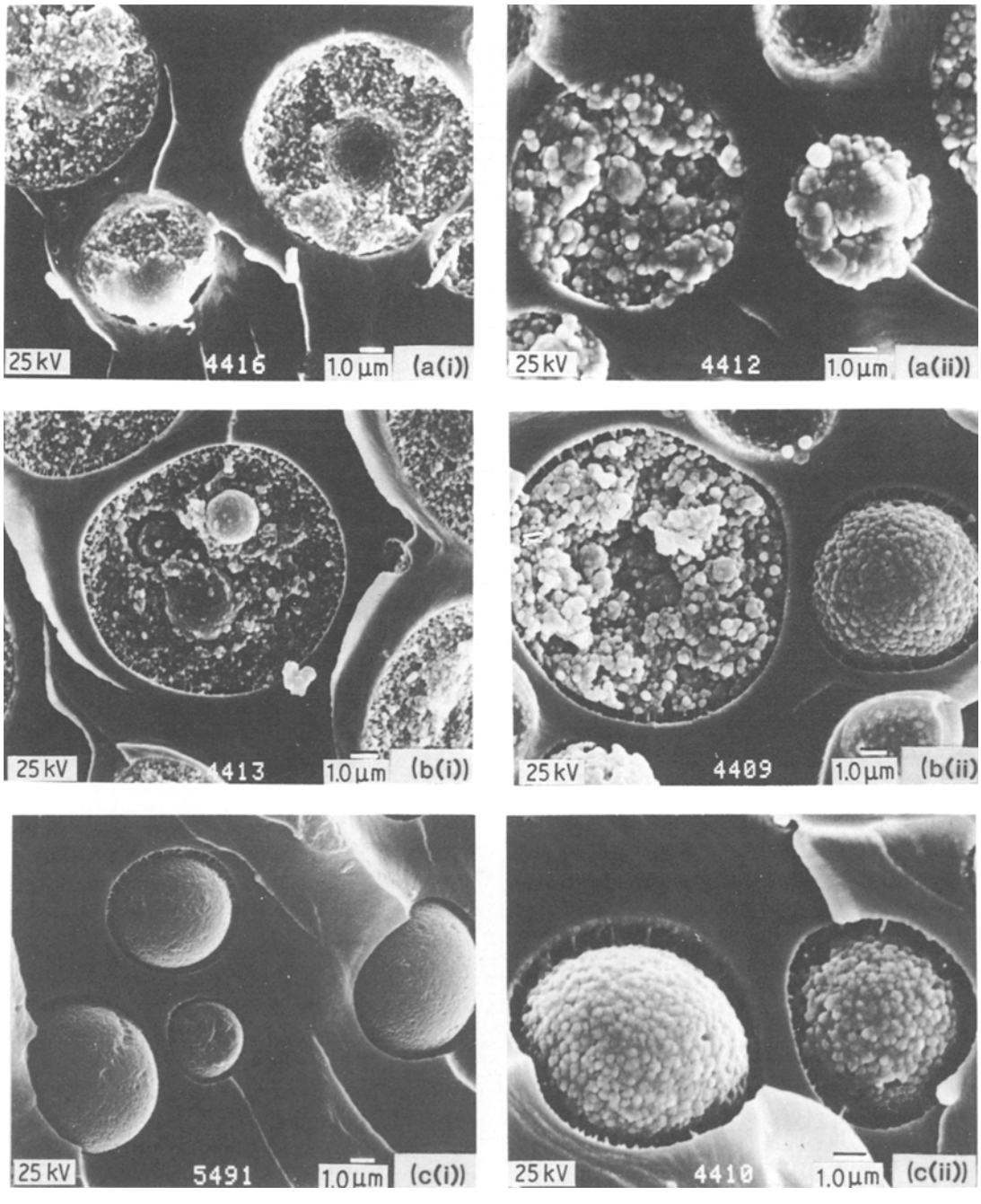

Figure 7 Scanning electron micrographs of DT fracture surface in polyester resins, modified with 9 pph CRC. Micrographs show (a) fast fracture zone, (b) arrest zone I, (c) arrest zone II. Resin systems are (i) C392 and (ii) C600PA.

particles seemed to have little effect upon the fracture path. Particles had fractured, and there was no evidence of plastic deformation, either in, or adjacent to the particles. In the arrest zone, a lot more surface features were visible, the fracture surface was rougher, and the particles were more readily distinguishable from the surrounding matrix. It is evident from Fig. 8c that plastic deformation has occurred in the rubber particles, but rather than being concentrated at the resin–matrix interface, the deformation was distributed throughout the particles, giving rise to consider-

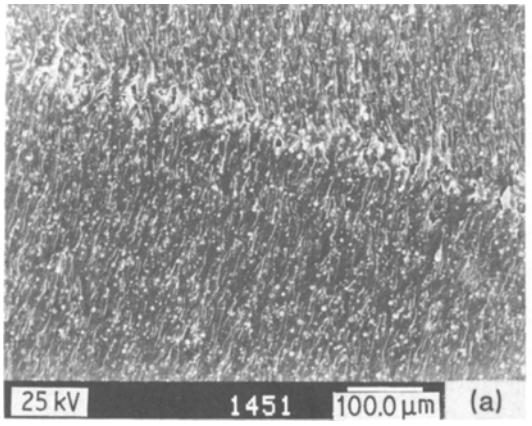

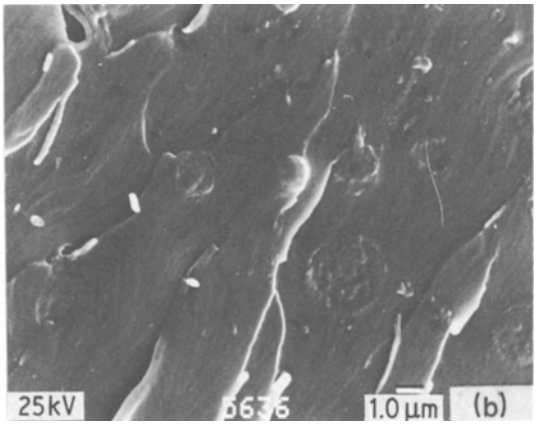

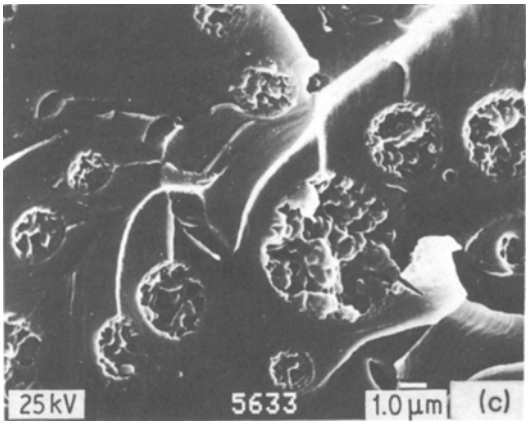

Figure 8 Scanning electron micrographs of DT fracture surface for C600PA + 3 pph CTBN. Micrographs show (a) low magnification view of fracture surface, (b) fast fracture, (c) crack arrest zone.

able internal cavitation. This voiding must have been associated with some increase in particle volume, during the deformation process.

Fig. 9 shows part of the DT fracture surface in C392 resin, modified with 10 pph CTBN rubber, and "hot-poured" to enhance rubber–resin compatibility in the uncured state (see Section 3.1.). The stress whitening in the arrest zone was more pronounced than at the lower CTBN rubber content, and the arrest zone was wider (around 700 μm). As with the other CTBN-modified resins examined, there was no visible division of the arrest zone. In the region of fast fracture (Fig. 9b), the fracture surface was considerably rougher than at lower rubber contents, and the rubber particles were more easily visible. The fracture path had passed directly through the particles, but there was no evidence of particle deformation, either within the particles or adjacent to them. Fig. 9c, which is at higher magnification than Fig. 9b, shows the fracture surface morphology in the region of crack arrest.

4. Discussion

4.1. Relationship between arrest markings and plastic zone

Fig. 5 shows that as the speed of DT testing decreases, the width of the arrest zone in regions of crack sticking increases, and evidence of plastic deformation (i.e. stress whitening) becomes more pronounced. If no crack propagation occurs during the load build-up which is associated with crack sticking, and if the crack propagates at high speeds only during periods of load drop, then the surface features seen in Fig. 5 must be associated with the zone of plastic deformation ahead of the crack tip.

Various expressions have been derived to calculate the size of the plastic deformation zone at crack tips but for relatively brittle and isotropic materials, the plastic zone radius (r_y), in plane strain, may be estimated by

$$r_y = \frac{1}{6\pi}\left(\frac{K}{\sigma_y}\right)^2$$

where K is the stress intensity factor and σ is the tensile strength [11].

In plane strain, the stress-intensity factor is related to the fracture surface energy (G) by the relation

$$K = \left[\frac{EG}{1-\nu^2}\right]^{1/2},$$

where E is Young's modulus and ν is Poisson's ratio (which has a value of around 0.35 for polyester resins). Thus knowing G, E and ν, r may be

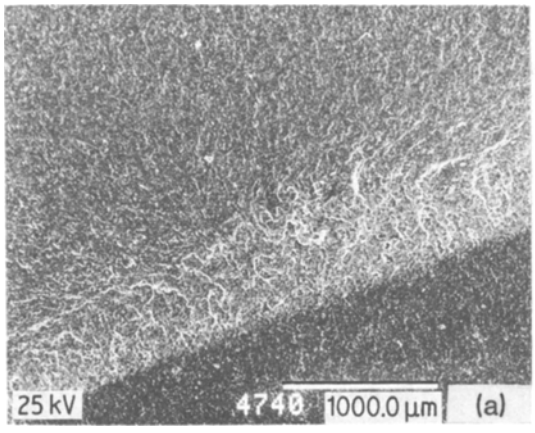

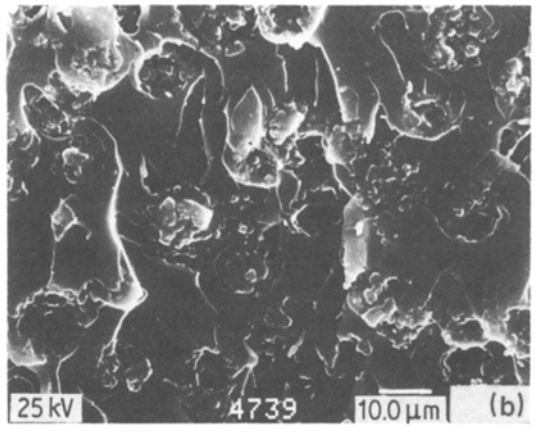

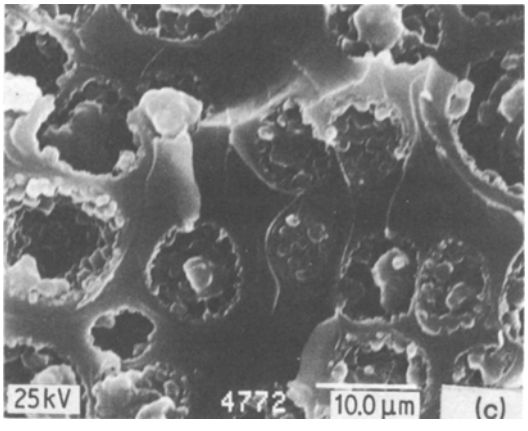

Figure 9 Scanning electron micrographs of DT fracture surface for C392 + 10 pph CTBN ("hot-poured"). Micrographs show (a) low magnification view of fracture surface, (b) fast fracture zone, (c) crack arrest zone.

calculated using the equation

$$r_y = \frac{1}{6\pi} \frac{EG}{(1-\nu^2)\sigma_y^2}.$$

The maximum value of the plastic zone radius ($r_{y,max}$) will be attained when G has its maximum value i.e. $G = G_i$, the fracture surface energy for crack initiation. Taking values of G_i, E and σ from tests described in Part I of this paper [6], $r_{y,max}$ was calculated for a range of testing speeds from 0.1 to 100 mm min^{-1}.

Table II lists calculated values of plastic zone radius, and measured values of arrest band width, for C392 resin with additions of 9 pph CRC1008 rubber tested over the range of crosshead speeds. The table clearly shows there is a large discrepancy between the size of the observed arrest regions, and the theoretically predicted plastic zone radius. In most cases, the arrest zone is around 40 times wider than the predicted plastic zone size. Such large and consistent variations between the two sets of data cannot be explained by experimental error, and it was therefore concluded that some low velocity "stable" crack growth had occurred, adjacent to the position of crack arrest, at all testing speeds. This conclusion is consistent with observations made by Phillips *et al.* [12] of slip–stick behaviour in untoughened epoxy thermosets. They showed that, subsequent to rapid crack propagation and arrest, slow crack growth occurred during specimen loading, resulting in a clearly defined slow growth zone being formed immediately ahead of the arrest line. In this region of slow growth, the crack-tip profile changed considerably. Immediately after crack arrest, the crack was observed to be sharp, but as loading was

TABLE II Comparison of calculated plastic zone sizes with width of arrest markings for C392 resin + 9 pph CRC 1008, DT tested at varying crosshead speeds

Crosshead speed (mm min^{-1})	σ_y (MPa)	G_i (J m^{-2})	r_y (µm)	Width of arrest markings (µm)
100	97	410	7	250
10	89	460	9	400
1	82	780	18	700
0.5	78	930	24	900
0.1	78	1235	32	1200

applied to it and slow crack growth occurred, the crack became more blunt, owing to plastic deformation at the crack tip. Stable crack propagation and associated crack blunting continued until a secondary sharp crack was initiated at the blunted crack tip. This secondary crack then propagated through the zone of plastic deformation formed at the blunted crack tip, prior to jumping rapidly through virginal material.

This description of slip–stick deformation in epoxy resin is in good qualitative agreement with the observations made by the authors, in rubber-toughened polyester resins. The decreased yield stress in the resin, resulting from the incorporation of second-phase rubber particles, meant that localized plastic deformation induced by stress concentrations adjacent to the crack tip, occurred at lower stress levels than in untoughened resin. Thus the crack blunting described by Phillips *et al.* occured more easily in toughened resin, and the tendency for slow crack growth to occur, in a stable manner, increased. Regions of slow crack growth are considered to correspond to the zone I regions of crack arrest observed in Fig. 5.

Observations of fracture features made by Phillips *et al.* and other authors [11] for unmodified thermosets do not, however, explain why the markings seen in the crack arrest zone in rubber-toughened polyesters are split into two distinct regions (Fig. 5). In unmodified resins, no equivalent feature to zone II of crack arrest is present (Fig. 5). This difference may be explained by comparing the yield behaviour of modified and unmodified thermosets. The unmodified material, which has a relatively high yield stress and low toughness, generates only a very small plastic zone ahead of the crack. Calculations of plastic zone size for unmodified polyester, based on data presented in Part 1 of this paper, gives values of plastic zone radius (r_y) of around 1 μm, at 1 mm min^{-1} testing speed. This is considerably smaller than any of the values calculated for rubber-toughened resin (Table II) even at much higher crosshead speeds, and would explain why zone II has not previously been observed in thermoset resins which fracture by slip–stick. In the toughened materials, however, the plastic zone size is calculated to be much larger, and it was concluded that zone II results from the secondary sharp crack, initiated at the blunted crack tip, propagating through the plastic zone ahead of the blunted crack, prior to rapid crack jumping through undeformed material. There is still, however, considerable quantitative discrepancy between the calculated values of r_y and the widths of arrest markings in Fig. 5, even when only zone II of crack arrest is considered. In all cases, the width of the late arrest zones considerably exceeded r_y.

4.2. Particle fracture morphologies

Figs. 6 and 7 show that, in CRC toughened resins, the rubber particles have distinct fracture morphologies in each of the three different regions of fracture that have been observed (fast fracture region, zones I and II). These fracture morphologies may be explained by considering the crack propagation mode occurring in each of the regions. In the zone of fast fracture, the crack front is travelling at velocities which may be in excess of 20 m sec^{-1} [11], and at these speeds there is no time for plastic deformation of the toughened material to occur, ahead of the crack tip. Therefore, there is no evidence of plastic deformation on the fracture surface, and the particles do not alter the fracture path.

In zone I of crack arrest, the fracture mode is completely different, and the crack front propagates at low crack speeds. This slow propagation allows plastic deformation to occur ahead of the crack tip, giving rise to a well-developed plastic zone, and associated stress whitening. Evidence of this plastic deformation around the particles is clearly visible in Fig. 7b. Cavitation around the rubber particles and formation of ligaments at the particle–matrix interface are clear evidence that yielding in the otherwise brittle matrix has been induced by the particles, since such features could not be generated if the resin behaved in a purely elastic manner. The fact that most of the particles in zone I have fractured indicates that the energy required to fracture the particles at low crack speeds is less than the energy required to cause fracture at the particle–resin interface.

In zone II of arrest zone, a secondary, sharp crack has initiated at the blunted crack tip, and this will be able to propagate at higher crack velocities through the resin as it has not been blunted. Initially, however, it has to pass through the plastic zone formed ahead of the blunted crack during slow propagation, before breaking through to undeformed material. It is this secondary propagation which, in the authors' opinion, gives rise to the second distinctive zone in the arrest region.

The material in this region has previously undergone plastic deformation, with its associated particle–matrix decohesion and ligament formation, but instead of being fractured by a slow moving, blunted crack front, a new sharp crack, moving at a higher velocity passes through the region. In this situation, the energy required to fracture the particles must be greater than that to cause failure at the already weakened particle–matrix interfaces, so the materials fail at the interface, giving the distinctive fracture appearances seen in Fig. 7c.

It is immediately apparent from Figs. 8 and 9, that the arrest zones in CTBN-toughened resins are different from those seen in CRC-toughened materials. There is no clearly visible division of the zones into two distinct regions, as may be seen in Fig. 5. This difference may be explained by considering the differences in deformation behaviour of the two types of particles. In plastically deformed CRC-toughened structures, cavitation occurs predominantly at the particle–matrix interface, with little internal deformation and voiding of the particles being apparent (Fig. 7). The two distinct modes of fracture described previously can thus operate. In plastically deformed CTBN-toughened resins, however, cavitation occurs throughout the particles, rather than being concentrated at the particle–matrix interface. It is not possible, therefore, for the fracture mode of particles in the arrest zone to change markedly, if a secondary, sharp crack propagates from the blunted crack tip, so no clear division of the stress whitened arrest zone is visible.

5. Conclusions

Electron microscopy has proved useful in investigating the fine structures and fracture modes of rubber-toughened polyester resins, Microscopy has shown that not all rubber additives investigated produce second-phase particle distributions, and that the fine structures of rubber domains which are produced are complex, and highly dependent upon both rubber and resin formulation, as well as rubber concentration.

Rubber additions modify the mode of fracture in polyester resins from continuous to slip–stick. Fractography provides an explanation for this change, as it reveals that rubber dispersions allow plastic deformation to occur ahead of cracks which have arrested or are travelling at low velocities, and crack blunting results. The reinitiation of a sharp crack from the blunted one produced a distinctive change in the fracture morphology in one rubber–resin system, and caused the arrest zone to be split into two distinctive regions.

Acknowledgements

Work described in this paper has been carried out by the authors in the School of Materials Science at the University of Bath, with funding from the Polymer Engineering Directorate of SERC. It is a pleasure to acknowledge the support and encouragement of PED. We should like to thank Scott Bader Ltd for the supply of resins and the experimental rubber system, and B. F. Goodrich Chemical Co for supplying their proprietary rubber additives. We also wish to thank Dr L. S. Norwood and Dr I. Alexander of Scott Bader for their advice and co-operation, and J. H. Crofton, formerly of the School of Materials Science, for his involvement in this work.

References

1. C. B. BUCKNALL, I. C. DRINKWATER and W. E. KEAST, *Polymer* **13** (1972) 115.
2. J. N. SULTAN and F. J. McGARRY, School of Engineering, M.I.T., Report R67-66 (1967).
3. J. N. SULTAN, R. C. LIABLE and F. J. McGARRY, *Appl. Polymer. Symp.* 6 (1971) 127.
4. E. H. ROWE and C. K. RIEW, *Plastics Engn.* **31** (3) (1975) 45.
5. W. D. BASCOM, R. L. COTTINGTON, R. L. JONES and P. PEYSER, *J. Appl. Polymer. Sci.* **19** (1975) 2545.
6. G. A. CROSBIE and M. G. PHILLIPS, *J. Mater. Sci.* in press.
7. C. K. RIEW and R. W. SMITH, *J. Polymer. Sci. Al* **9** (1971) 2739.
8. E. H. ROWE, Proceedings 34th Annual Technical Conference, S.P.I. RP/C Institute (1979) 23-B.
9. P. D. TETLOW, J. F. MANDELL and F. J. McGARRY, *ibid.*, 23-F.
10. C. B. BUCKNALL, "Toughened Plastics" (Applied Science, London, 1977).
11. A. J. KINLOCH and R. J. YOUNG, "Fracture Behaviour of Polymers" (Applied Science, London, (1983).
12. D. C. PHILLIPS, J. M. SCOTT and M. JONES, *J. Mater. Sci.* **13** (1978) 311.

Received 18 January
and accepted 10 April 1984